Special Issue on "Theoretical and Computational Chemistry"

J. Indian Chem. Soc.,
Vol. 96, July 2019, pp. 825-836

Comparative oxidative ability of iron(III)-iodosylarene vs. high-valent iron(IV/V)-oxo species: Is lower oxidation state a key to enhance selectivity in organic transformations?

Ravi Kumar, Bhawana Pandey and Gopalan Rajaraman*

Department of Chemistry, Indian Institute of Technology Bombay, Powai, Mumbai-400 076, India

E-mail: rajaraman@chem.iitb.ac.in

Manuscript received online 22 April 2019, revised and accepted 15 May 2019

High-valent iron(IV/V)-oxo species are known as the potent oxidant in various organic transformations such as C-C, C-H activation reactions. While the aggressive oxidative abilities of these species are established, very little is known about the oxidative abilities of the precursor complexes that generate these species. This is particularly important, as often these species are not generated with 100% conversion and present a possibility with the coexistence of the catalytic precursor in the solution. Given this background, it is important to establish the comparative oxidative ability of the precursor materials viz a viz iron(IV/V)-oxo species. In our current study, along with high-valent iron(IV/V)-oxo species, we have also tested the reactivity of the iron(III)-iodosylarene towards epoxidation reaction. DFT methods have been taken into account to establish a detailed mechanism of this reaction. A comprehensive study of the mechanism of epoxidation of styrene reveals that the energetic requirement of generating the iron(IV/V)-oxo species from the iron(III)-iodosylarene is on par with the direct olefin epoxidation by the iron(III)-iodosylarene. As there are additional barriers for the high-valent oxo species to activate olefin, it is safe to conclude iron(III)-iodosylarene as the potent oxidant in this reaction. A careful electronic structure analysis reveals that ligand design is playing a major role in tuning the reactivity of the iron(III)-species hence altering the entire landscape of the catalytic transformations. This work unequivocally establishes that Fe(III)-iodosylarene as a powerful oxidant. Since this act as a key catalytic precursor for the formation of Fe^{IV}=O species, this likely to trigger an intense debate on the need to evoke aggressive oxidant such as Fe^{IV}=O in other catalytic transformations.

Keywords: Iron(III)-iodosylarene, iron(IV/V)-oxo, reactivity, epoxidation, DFT.

Introduction

Heme and non-heme metalloenzymes are known as efficient and robust catalysts for reactions such as hydroxylation, epoxidation and C-H activation of aliphatic/aromatic hydrocarbons[1]. The active site of these metalloenzymes contains high-valent metal-oxo, peroxo or superoxo species that are known to be aggressive oxidants towards inert substrates[2]. This has triggered the interest in bio-mimick chemistry where high valent metal-oxo, peroxo and superoxo complexes mimicking the active site structure of enzymes are prepared as structural-functional models of enzyme and have been employed extensively in several catalytic transformation[3]. Although quite a few high-valent metal-oxo complexes are spectroscopically detected and for some even X-ray structures are available, their catalytic selectivity, efficiency, and robustness are diverse and the catalytically active species is often elusive leading to various proposals and ambiguities[4].

Among, high-valent metal-oxo complexes, iron-oxo complexes play an important role in biological chemistry[1]. In the iron-oxo species, Fe^{IV}=O species is well known in the cytochrome P450 enzyme which efficiently catalyzes various types of metabolic reactions such as oxidation, reduction, isomerization as well as dehydration[5]. To mimic the reactivity of this species, ceaselessly numerous synthetic efforts have been undertaken. Over several decades, significant advancements towards the direct characterization of heme and non-heme Fe^{IV}=O and Fe^{V}=O have been performed[4]. Some of the ligands which stabilize the Fe^{IV}=O and Fe^{V}=O species are shown in Fig. 1. The detailed structural knowledge on these model complexes such as, $[(TMCS)Fe^{IV}=O]^{+}$ (TMCS = 1-mercaptoethyl-4,8,11-trimethyl-1,4,8,11-tetrazacyclotetradecane)[6], $[(TAML)Fe^{V}=O]^{-}$ (TAML = tetraamido macrocyclic ligand)[4b] and $[(14\text{-}TMC)Fe^{IV}=O]^{2+}$ (14-TMC=1,4,8,11-tetramethyl-1,4,8,11-tetraazacyclotetra-

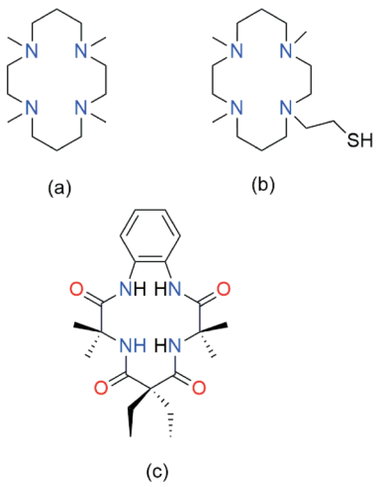

Fig. 1. Schematic representation of some widely used ligands in non-heme complexes: (a) 14-TMC, (b) TMCS and (c) TAML.

decane)[4a] are available now as thorough experimental and spectroscopic studies have been undertaken.

Initially, from the economical points of view, molecular oxygen (O_2)[7] and hydrogen peroxide (H_2O_2)[8] are the oxidants of choice. In 1979, Groves and co-workers for the first time used iron(III)-porphyrin with iodosylarene (PhIO) for the oxidation of hydrocarbon[9]. After that many groups have focused on the use of PhIO as an artificial oxidant in metal-catalyzed oxidation reactions[10]. While this species is widely used to generate the putative Fe^{IV}=O species, this involves cleavage of I···O bond. A recent report suggests a possibility of utilizing the iodosylarene species itself as an oxidant emerge and experimental evidence gathered in this direction clearly dictate the possibility of this species rather than the high-valent Fe-oxo species as an active oxidant[11]. Particularly, report of iron(III)-iodosylbenzene complexes as a reactive intermediate instead of high-valent Fe^{IV}=O and Fe^{V}=O utilizing 13-TMC ligand gather wide attention and speculate this possibility also in other catalytic reactions where in general iron(III)-iodosylbenzene has been utilized as a catalytic precursor. In this work, the reactivity of [(13-TMC)Fe^{III}-OIPh]$^{3+}$ (13-TMC=1,4,7,10-tetramethyl-1,4,7,10-tetraaza-cyclotridecane) (see Fig. 2) and its derivatives with [(13-TMC)Fe^{IV}=O]$^{2+}$ has been compared to arrive at the aforementioned conclusions.

Computational tools play an important role in establishing the reaction mechanism of such intricate reactions in general. As various spin-states are involved, very often identifying the nature of the catalyst is challenging and theoretical tools combined with the gather experimental evidence can provide insight into the nature of the catalytic species. In our current study, we aim to utilize density functional methods to achieve the following (i) to understand the electronic structure of the iron(III)-iodosylarene, (ii) to establish the nature of oxidant among iron(III)-iodosylarene, Fe^{IV}=O and Fe^{V}=O species in olefin epoxidation.

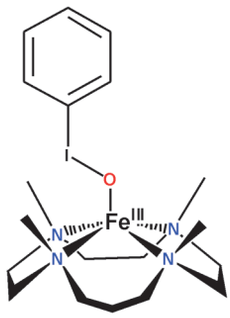

Fig. 2. Schematic representation of [(13-TMC)Fe^{III}-OIPh]$^{3+}$ (**1**).

Computational details

In the present work, previously established procedures are used for all the calculations[12]. Here, the geometry optimizations were done using the Gaussian 09[13], suite of program and spectroscopic parameters are calculated with the ORCA 3.0.3 program package incorporating COSMO solvent effect[14]. All the reported geometries were optimized using the Grimme's dispersion corrected unrestricted B3LYP functional (UB3LYP-D2)[15]. A double ζ-quality basis set with the Los Alamos effective core potential (LANL2DZ ECP) for Fe[16], LANL2DZdp ECP for I (where dp stands for polarization function of d symmetry and diffuse functions of p symmetry)[12b] and a 6-31+G* basis set for C, H, O, N[12f] for geometry optimization and frequency calculations were chosen. This is followed by single-point energy calculations using a TZVP[12a,12c,17] basis set for C, H, O, N, Fe and I with SDD ECP on the optimized geometries[18]. The minima (lowest energy geometry) and first-order saddle point (transition state) on the potential energy surface (PES) are verified using frequency calculation and it gave also the zero point as well as free energy corrections on the electronic energies of optimized geometry. The quoted DFT energies are UB3LYP-D2/SDD(I),TZVP(rest)//UB3LYP-D2/LanL2DZ(Fe), Lan-

L2DZdp(I), 6-31+G*(rest) solvation including free-energy corrections at the temperature of 298.15 K, unless otherwise mentioned. Calculations were performed using acetonitrile as solvent using the polarizable continuum model (PCM)[19]. Spin density visualizations are done using chemcraft software[20]. All the energies reported in the paper are zero-point corrected solvation energies (ΔE). Time-dependent density functional theory (TD-DFT) calculations were performed using the ORCA program, incorporating relativistic effects by the zeroth-order regular approximations methods (ZORA)[21] at B3LYP/TZVP level of theory. Natural bond order (NBO) analysis is carried out using Gaussian 09[22]. While basis set superposition error could play a role in the estimated energetics, at various occasion these effects are known to be small and hence has not been computed here[23].

Results

Electronic structure of [(13-TMC)Fe^{III}OIPh]$^{3+}$ (1)

Since Fe(III)-iodoylarene [(13-TMC)Fe^{III}OIPh] (**1**) has been proposed as a putative oxidant in the olefin epoxidation reaction and its electronic structure details are previously not known, we would like to begin with establishing the electronic structure of this species here. The iron(III) center here has three different spin possibilities viz. sextet (S=5/2), quartet (S=3/2) and doublet (S=1/2) states. Among all three possible spin states, DFT calculations predict the sextet state (^{6}**1**) as the ground state and quartet and doublet found to lie at 10.1 and 88.0 kJ/mol higher in energy, respectively. Optimized structure of the ground state of **1** and its corresponding spin density plot is shown in Fig. 3. Geometry around Fe^{III} center is distorted square pyramidal which is exhibiting a deviation of 0.805 from an ideal square pyramidal geometry (using SHAPE software[24]). The Fe^{III}-O bond length is computed to be 1.822 Å which corresponds to a single covalent bond while O-I and Fe-N$_{av}$ (average of all four Fe-N distances) bond lengths are 1.985 Å and 2.190 Å, respectively (see Table S1).

These bond lengths parameters are in accord with the data reported earlier for heme models based on cytochrome P450[25]. Spin density of 4.099 has been detected on the iron center while oxygen and nitrogen atoms gain spin densities due to spin delocalization. Here, we see that the maximum unpaired electron spin densities are located on Fe and O atoms and the rest delocalized on the 13-TMC ring nitrogens (see Table S2).

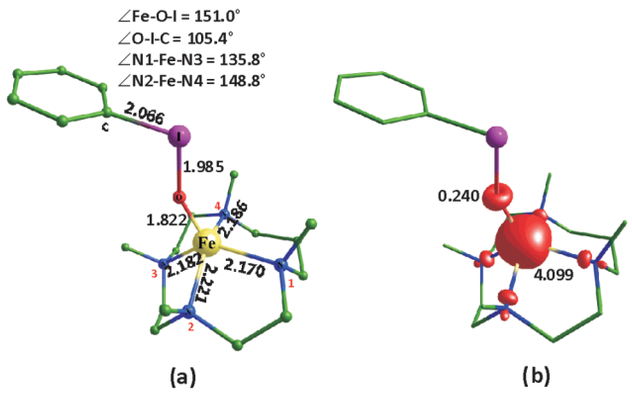

Fig. 3. B3LYP-D2 (a) optimized geometry of ground state of [(13-TMC)Fe^{III}-OIPh]$^{3+}$ (**1**) and (b) its corresponding spin density plot. All the bond lengths are given in Å and bond angles are in degree (°). Spin density plot are presented with a contour value of 0.03 a.u. and values shown are in arbitrary units.

The electronic configuration for the ground state (S=5/2) of complex **1** is computed to be $(\delta^*_{xy})^1(\pi^*_{xz})^1(\pi^*_{yz})^1$ $(\sigma^*_{x^2-y^2})^1$ $(\sigma^*_{z^2})^1$ (see Fig. 4). From the below figure, it is clear that the non-bonding δ^*_{xy} orbital is found to be the most stabilized one. The π^* set of orbitals viz. π^*_{xz} and π^*_{yz} orbitals are high

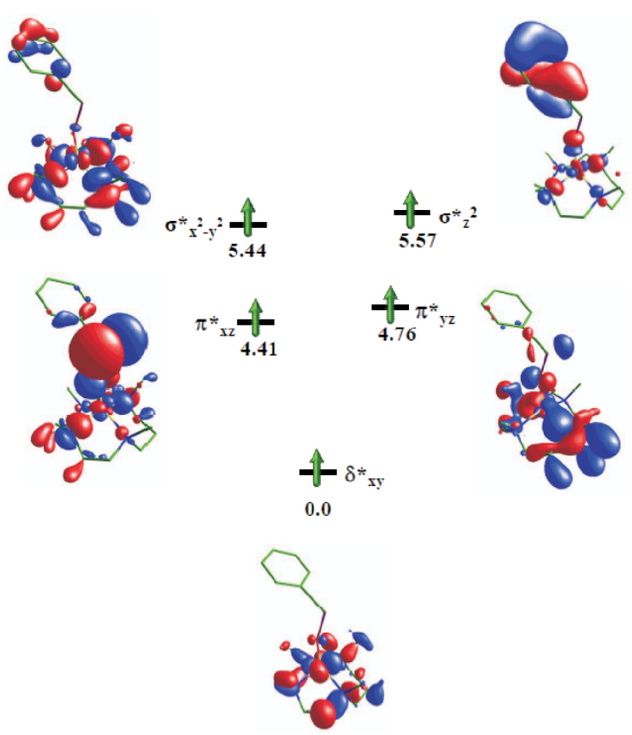

Fig. 4. Electronic structure and molecular orbitals of the ground state (S=5/2) of the complex **1**. All the relative energies of molecular orbitals are given in eV.

lying with 4.41 and 4.76 eV, respectively. The $\sigma^*_{x^2-y^2}$ and $\sigma^*_{z^2}$ orbitals are nearly degenerate with a smaller energy gap of 0.13 eV.

To understand the bonding in **1**, a detailed NBO analysis has been performed. The NBO analysis reveals that Fe-O σ-bonding interaction is composed of a 13.86% of Fe(d_{z^2}) and 86.14% of O(p_z) orbitals while π-bonding interaction composed of a 13.33% of Fe(d_{xz}) and 86.76% of O(p_x) orbitals (see Fig. 5). Both the bonds are found to be strongly ionic in character with a significant donation from the oxygen atoms. Additionally, the O-I σ-bond is formed by 71.44% contribution from O(p_y) and 28.56% contribution from I(p_y). These observations suggest that Fe-O bond and O-I bonds are ionic in nature. The Wiberg bond index (WBI)[26] values for Fe-O and O-I bonds are 0.53 and 0.69 both suggestive of a net single bond.

To comprehend the electronic structure of complex **1** further, we have computed the corresponding spectral features. Particularly, we have computed the absorption spectra using TD-DFT and the computed absorption spectra using acetonitrile as a solvent for the ^{6}**1** state shows two characteristic peaks at 616 nm and a broad peak centered at 821 nm. Both these peak positions are in agreement with the experiments (shown in Fig. 6 as a solid black line). The peak observed at 616 nm is found to be due to the transition of π*{(Fe-O)-IPh} moiety to the $d_{x^2-y^2}$ orbitals of the iron.

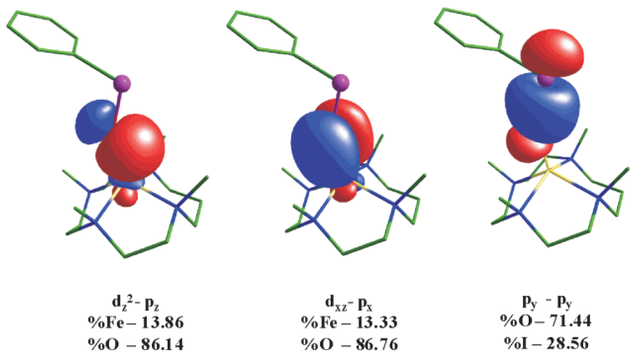

Fig. 5. NBO diagram for selective bonds for the ground state of **1** showing σ-bonding and π-bonding interaction between Fe^{III}, O and I atoms of Fe-O-I moiety.

Another peak computed at 821 nm shows d-d transition from π* (Fe_{dxy}-O_{px}) to σ* (Fe_{dz^2}-O_{pz}) orbitals. Experiments also reveal a broad feature around this region offering confidence on the computed electronic structure parameters.

Reactivity studies of complex 1 towards the epoxidation of styrene

To understand the reactivity of complex **1** towards C=C bond activation, we have chosen a well-known substrate styrene and tested its reactivity towards the epoxidation reaction. Various plausible reaction pathways have been explored (see Scheme 1). Three possible pathways are proposed and among these pathways, the first pathway (pathway a) involves

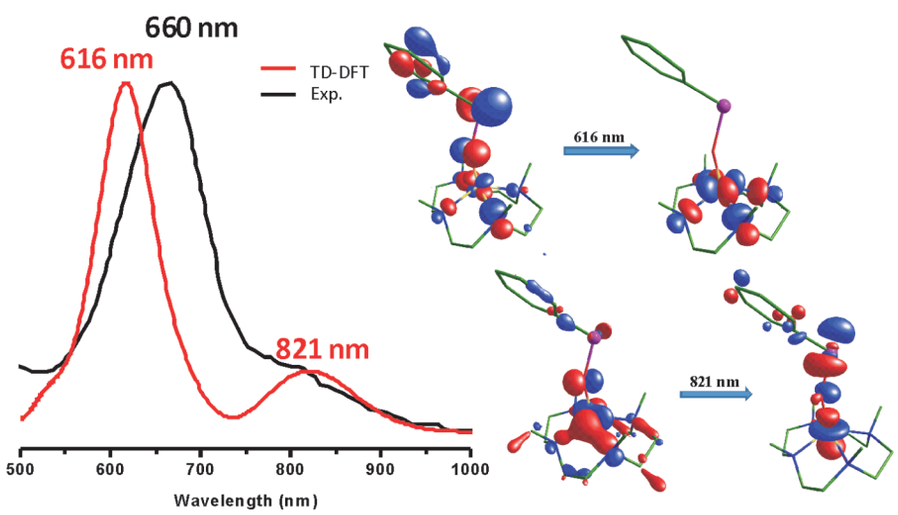

Fig. 6. Absorption spectra computed using TD-DFT calculations on the ground state of complex **1** and its corresponding orbitals involved in the transitions. The experimental spectrum of **1** obtained from Ref. 11 is given in black line for comparison[11].

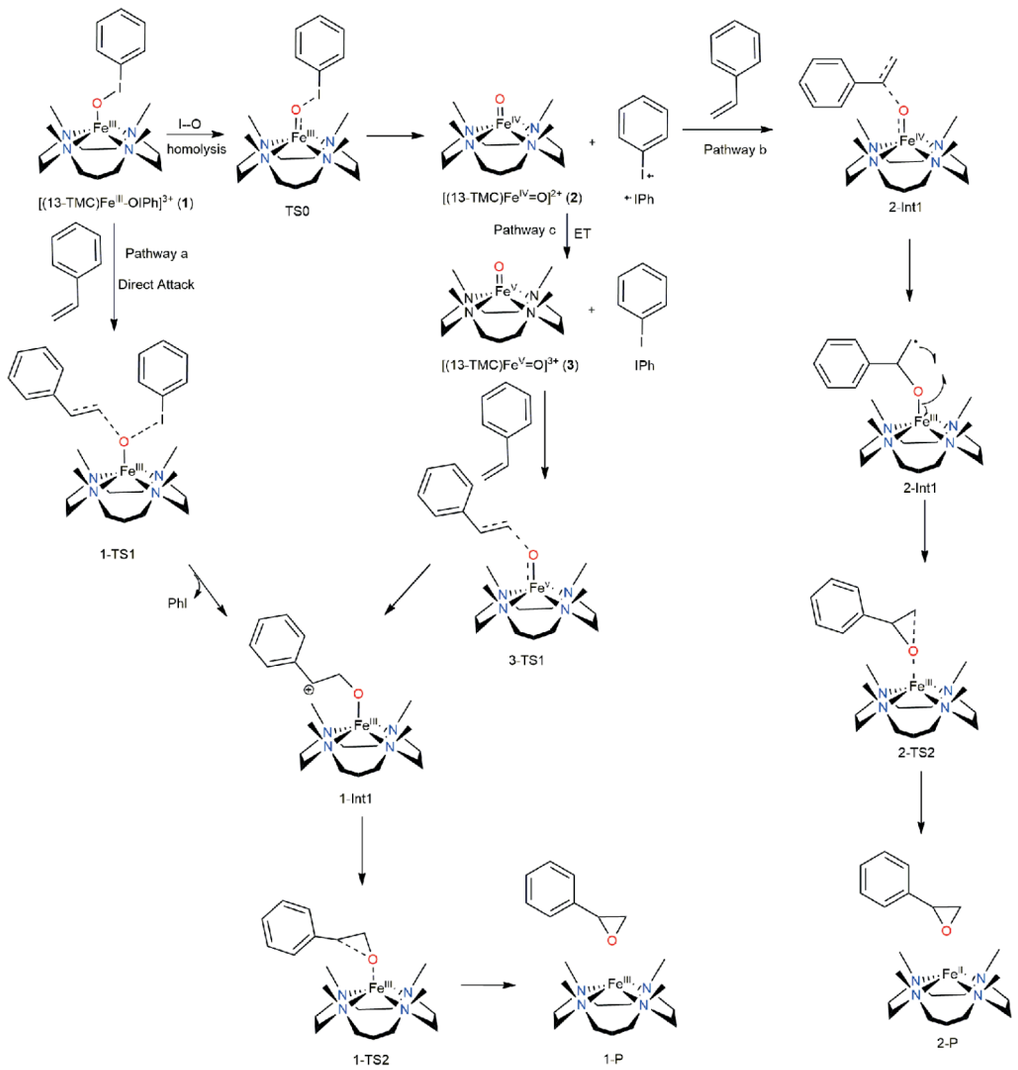

Scheme 1. Various possible reaction pathways for the epoxidation of styrene starting from [(13-TMC)Fe^{III}-OIPh]$^{3+}$ (**1**).

the direct attack on styrene by iron(III)-iodosylarene complex **1**, leading to the formation of intermediate 1 (**1-Int1**). The other two pathways involve a common first step viz. homolytic cleavage of the O···I bond to generate Fe^{IV}=O species [(13-TMC)Fe^{IV}=O]$^{2+}$ (**2**) along with highly reactive iodobenzene cation radical (PhI$^{+\bullet}$). In the next step, either species **2** can directly attack the styrene to generate a product via a radical intermediate (**2-Int1,** pathway b) or species **2** can undergo further oxidation and donate one electron through electron transfer mechanism (ET) to the iodobenzene radical cation leading to the formation of the putative [(13-TMC)Fe^{V}=O]$^{3+}$ (**3**) species and iodobenzene (pathway c, see Scheme 1 for details). In the subsequent steps, species **3** can attack styrene to form the epoxidation product via intermediate **3-Int1** (see Scheme 1).

Direct attack of styrene on iron(III)-iodosylarene complex 1 (pathway a)

In this pathway, a styrene molecule is expected to be directly attacked by the iodosylarene complex **1** via **1-TS1** to form intermediate **1-Int1** with a newly formed O-C bond. We have computed all the three possible spin states (S=5/2, 3/2 and1/2) for the transition state (**1-TS1**) corresponding to the direct C=C bond activation. Computed potential energy surface for the epoxidation reaction of complex **1** is shown in Fig. 9. The calculated barrier heights for sextet, quartet, and

doublet states are found to be 53.6, 66.2 and 147.1 kJ/mol, respectively. The sextet state found to have the lowest activation energy and hence no spin crossover to other spin states are desired in this reaction pathway. From the computed barrier heights, it is evident that S=1/2 state has no role on the reactivity as this surface lie very high in energy compared to the other two spin states. The approach of styrene C1 carbon towards the oxygen of Fe^{III}-OIPh moiety of **1** in transition state (**^{6}1-TS1**) is apparent from the decrease in O···C1 bond distance [1.935 Å] and simultaneous increase in Fe···O [2.115 Å], O···I [2.009 Å] and C1···C2 distances [1.409 Å], which is characterised by the imaginary frequency of *i*370 cm^{-1} (Fig. 7).

Spin density at the iron and oxygen centers for the energetically low-lying transition state (**^{6}1-TS1**) are found to be 3.846 and 0.113, respectively (see Fig. 7(a) and (b)). These spin density values are slightly reduced compared to the same in **^{6}1** reactant (Fe=4.099 and O=0.240). The alpha HOMO of the **^{6}1-TS1** reveals that the π orbital of the styrene are donating the electrons into the O-I orbital leading to the likely cleavage of the O···I bond in the next step (see Fig. 7(c)).

For intermediate (**1-Int1**) also sextet state is found to be the ground state, with quartet state lying at 24.0 kJ/mol higher in energy. Thermodynamically, the formation of this intermediate (**^{6}1-Int1**) is found to be highly exothermic in nature by 224.4 kJ/mol suggesting the feasibility of the formation of this intermediate in the reaction. Spin density analysis clearly reveals the absence of any radical character on the C2 carbon atoms and charge analysis indicate that this species is rather cationic than a radical intermediate (see Fig. 8). In the next step, the ring closure transition state followed by the formation of the product is expected. Since there is a significant gain in stabilizing the cationic intermediate and it is very well known that the ring closure transition states are often barrier-less[27] or have a very small barrier, we expect that the reaction proceeds smoothly upon the formation of the intermediate leading to the desired epoxide product.

Formation of Fe^{IV}=O species and its reactivity towards styrene (pathway b)

The I-O bond can undergo either homolytic or heterolytic cleavage to form Fe^{IV}=O or Fe^{V}=O species, respectively. Earlier experimental reports suggest homolytic cleavage of the I···O bond and support the formation of Fe^{IV}=O species (**2**). The homolytic cleavage of the I···O bond is expected to occur via **TS0** from species **1** leading to the formation of species **2**. Here we have computed the sextet and quartet

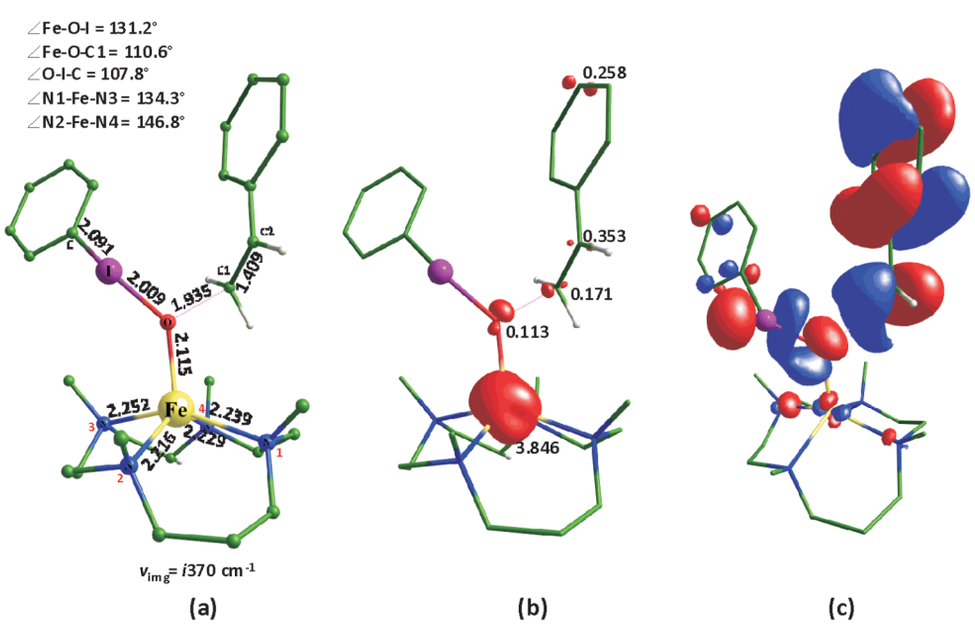

Fig. 7. B3LYP-D2 (a) optimized geometry of the lowest transition state (**^{6}1-TS1**), (b) its corresponding spin density plot and (c) alpha HOMO orbital picture. Spin density plot and alpha HOMO orbital picture are presented with a contour value of 0.03 a.u.

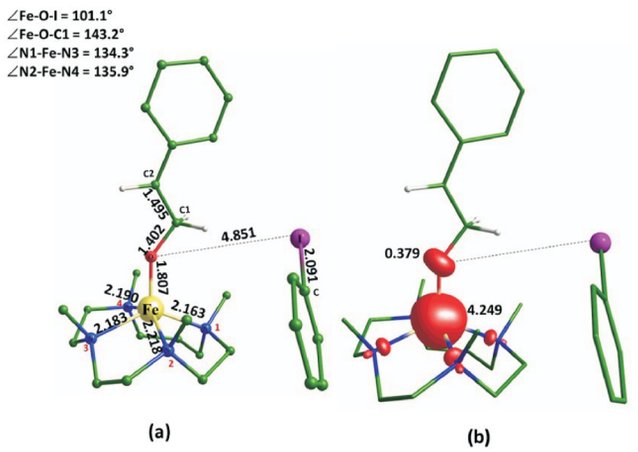

Fig. 8. B3LYP-D2 (a) optimized geometry of ground state of ^{6}**1-Int1** and (b) its corresponding spin density plot. All the bond lengths are given in Å and bond angles are in degree (°).

transition states and our calculations suggest that ^{4}**TS0** being lowest lying with an estimated barrier of 51.4 kJ/mol followed by ^{6}**TS0** state at 67.3 kJ/mol (see Fig. 11). This suggests a possible spin-crossover from the ^{6}**1** state to ^{4}**TS0** state during the course of the reaction. The transition state (^{4}**TS0**) exhibited a characteristic imaginary frequency of *i*262 cm^{-1} corresponding to a significant decrease of Fe···O distance from 1.864 Å (^{4}**1**) to 1.690 Å (^{4}**TS0**), along with simultaneous increased I···O bond distance from 1.966 Å (^{4}**1**) to 2.358 Å (^{4}**TS0**), depicting the dissociation of O···I bond. The spin density on Fe, O and I are found to be 2.187, 0.236 and 0.376 respectively (see Fig. 10). The combined spin density on PhI moiety is 0.744 which suggests the formation of $PhI^{\bullet+}$ upon cleavage of the O···I bond leading to the formation of Fe^{IV}=O species. This is also confirmed with the Intrinsic Reaction Coordinate (IRC) calculations (see Supporting Information). Furthermore, significant spin densities at the oxygen and Iodine atoms also affirm homolytic cleavage of the O···I bond leading to the formation of species **2**.

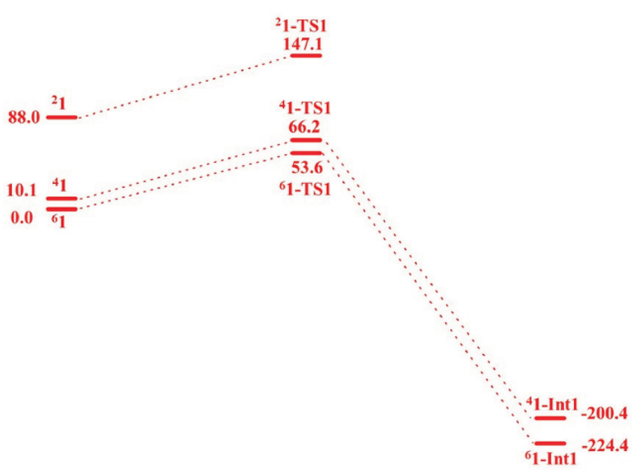

Fig. 9. B3LYP-D2 computed potential energy surface (ΔE in kJ/mol) for epoxidation of styrene by [(13-TMC)Fe^{III}-OIPh]$^{3+}$ (**1**).

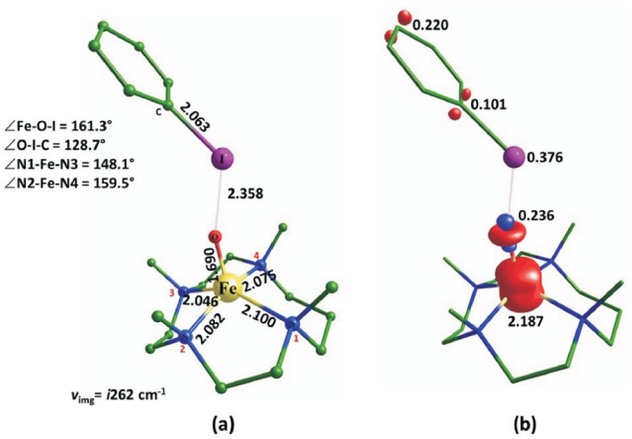

Fig. 10. B3LYP-D2 (a) optimized geometry of lowest transition state ^{4}**TS0** and (b) its corresponding spin density plot. All the bond lengths are given in Å and bond angles are in degree (°).

The formation of Fe^{IV}=O [(13-TMC)Fe^{IV}O] (**2**) from **1** is found to be endothermic in nature by 34.6 kJ/mol in energy. The ground state for species **2** is found to be triplet spin state (^{3}**2**) with quintet excited state (^{5}**2**) found to lie at 29.5 kJ/mol higher in energy. The Fe-O bond is decreased to 1.587 Å in ^{3}**2** compared to transition state ^{4}**TS0** (1.690 Å) which suggests the formation of Fe=O double bond character (see Fig. 12). The spin density on Fe and O are found to be 1.342 and 0.715, respectively, revealing characteristic oxyl-radical character on the oxygen atom as witnessed for this species earlier[12a,12c].

The Fe^{IV}=O species (**2**) reacts with styrene at C2 carbon through **2-TS1**. Here we could compute only triplet spin state (^{3}**2-TS1**) which has an energy barrier of 67.4 kJ/mol and quintet transition state was not converging correctly with the desired spin state despite several attempts. However, given the substantial triplet-quintet gap (~34.3 kJ/mol) and a fact that ^{3}**2-TS1** transition found to lie 1.5 kJ/mol lower in energy

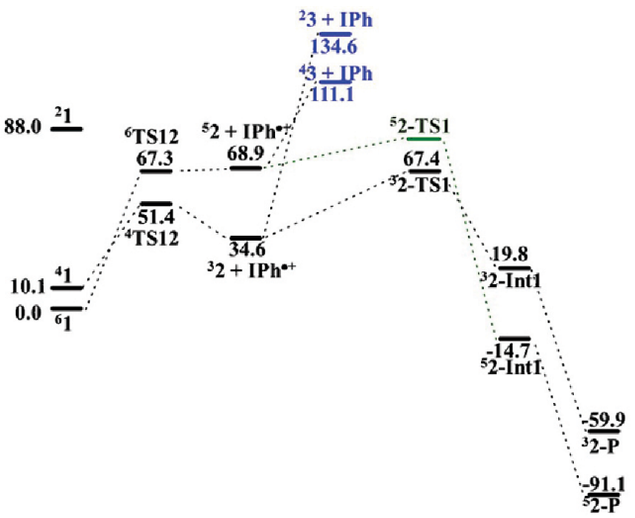

Fig. 11. B3LYP-D2 computed potential energy surface (ΔE in kJ/mol) for epoxidation of styrene involving pathways b and c through [(13-TMC)Fe^{III}-OIPh]$^{3+}$ (**1**). Black and blue lines show various pathways viz. b and c pathways depicted in Scheme 1. Pathway b depict the formation of Fe^{IV}=O species and its reactivity in activating the styrene and pathway c depict the formation energy required for the generation of putative Fe^{V}=O species. **^{5}2-TS1** in the green line indicates a possible transition state that could connect the intermediate to the product but this has not been converged correctly to the desired spin states.

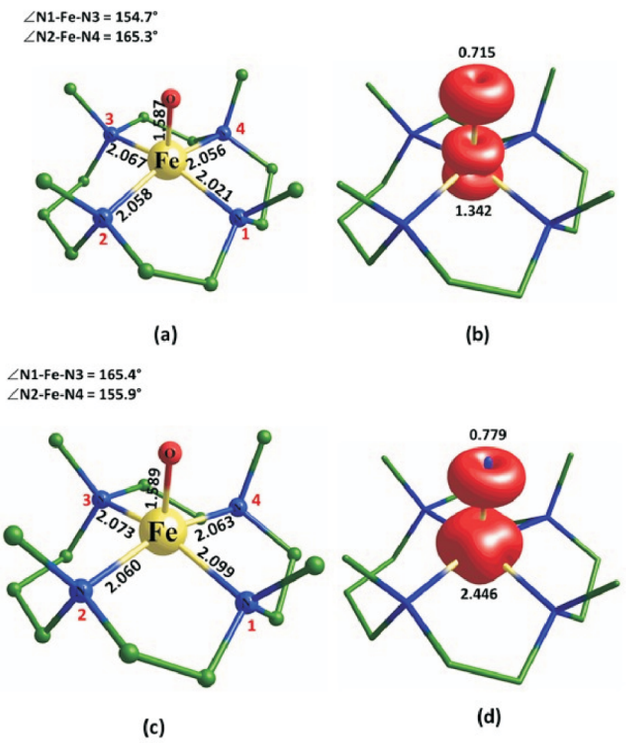

Fig. 12. B3LYP-D2 (a) optimized geometry of ground state of **^{3}2**, (b) its corresponding spin density plot, (c) optimized geometry of ground state of **^{4}3** and (d) its corresponding spin density plot.

compared to **^{5}2** reactant suggests that the quintet reactivity, as often invoked in the reactivity of Fe^{IV}=O, is unlikely to alter the reactivity pattern computed. This also rationalizes rather a sluggish reactivity observed for this species towards various substrates such as styrene. While the barrier computed for the C=C activation at the triplet surface is not substantial, this is likely to hinder the formation of the epoxide, if species **2** to be generated from **1** as there is already a substantial barrier for the cleavage of the O···I bond. This is also supported by the experiment that *in situ* generated Fe^{IV}=O species found to be unreactive towards styrene. Spin density computed at the **^{3}2-TS1** reveal a spin density of –0.608 on the C1 carbon atom and this clearly suggests the possibility of the radical pathway for the epoxidation reaction as has been observed generally in the reactivity of Fe^{IV}=O species (see Fig. 13)[6,9,10,28]. In the next step, the formation of **2-Int1** has been assumed to take place. Here quintet state is found to be the ground state with the triplet state found to lie 34.7 kJ/mol higher in energy. This suggests a possible spin-crossover post **^{3}2-TS1** formation leading to **^{5}2-Int1** species (see Fig. 13). The shortening in O···C2 bond distance [1.974 Å to 1.455 Å] with a simultaneous increase in Fe···O [1.709 Å to 1.792 Å] and C1···C2 [1.396 Å to 1.482 Å] is evident with an imaginary frequency of *i* 276 cm^{-1}. In the intermediate **^{5}2-Int1**, the O-C2 bond distance is found to be 1.460 Å which corresponds to an O-C single bond and spin density on C1 carbon now found to be –1.022 which shows the presence of one unpaired β-electron on this carbon center. This intermediate in the next step expected to undergo a ring closure transition state leading to the formation of the epoxide product. As this ring closure transitions states are often a barrier-less process, we have not attempted to compute these additional steps. In the final step, the formation of the epoxide and Fe(II)TMC is assumed and here quintet state **^{5}2-P** is found to be lower in energy compared to the triplet state **^{3}2-P** by 31.2 kJ/mol.

Formation of Fe^{V}=O species (Pathway c)

Since the cleavage of the O···I bond is found to be exclusively homolytic in all the spin surface computed, the forma-

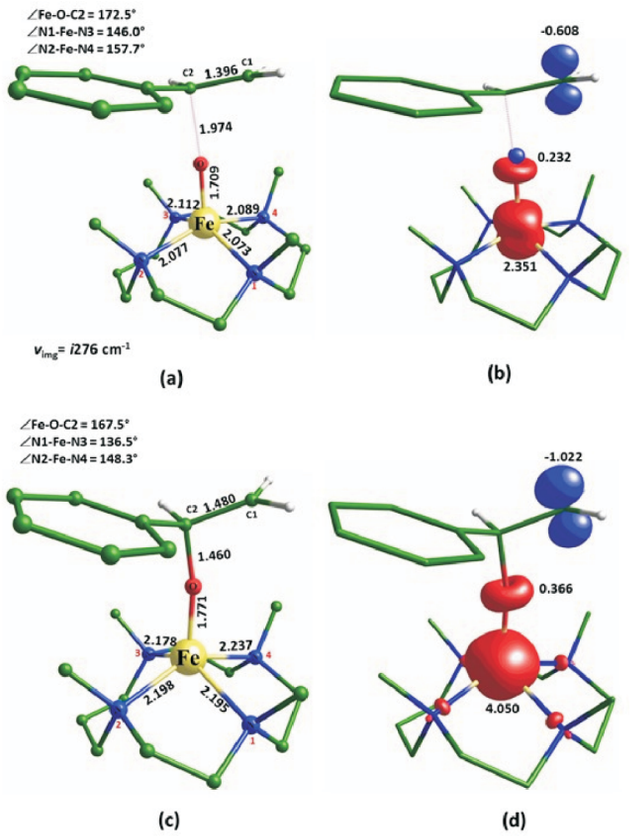

Fig. 13. B3LYP-D2 (a) optimized geometry of lower transition state of ^{3}**2-TS1**, (b) its corresponding spin density plot, (c) optimized geometry of ground state of ^{5}**2-TS1** and (d) its corresponding spin density plot.

tion of putative Fe^{V}=O is not expected under the experimental conditions undertaken. Alternative ways to the formation of Fe^{V}=O involves further oxidation of species **2** by an electron transfer from this species to the $PhI^{\bullet+}$ species. An intermolecular electron transfer from **2** to $PhI^{\bullet+}$ expected to form [(13-TMC)Fe^{V}O] species (**3**). In the case of **3**, quartet spin state (^{4}**3**) is found to be the ground state with 23.5 kJ/mol energy with respect to the doublet spin state (^{2}**3**). As the formal oxidation state increases from IV to V, the Fe-O bond distance decreases from 1.603 Å to 1.589 Å as we go from ^{5}**2** to ^{4}**3** species. Similarly, a shortening of Fe=O bond is witnessed also in the quintet surface (^{5}**2** 1.587 Å vs ^{4}**3** 1.528 Å). These changes in Fe=O bond distance with increasing in oxidation state are within our general expectations for such species[29]. The spin density of the unpaired electron is predominantly delocalized in Fe-O bond of ^{4}**3** (Fe=2.446 and O=0.779). The conversion of **2** to **3** is found to be significantly endothermic process by 76.5 kJ/mol energy from low lying intermediate **2** (^{3}**2**). This observation suggests that the formation of **3** from **2** is thermodynamically not feasible and this rules out the formation of Fe^{V}=O species in this reaction mixture and this is supported by the experiments[11].

Discussion

Generally, it is found that high-valent Fe^{IV}=O and Fe^{V}=O species formed by O···I bond cleavage from Fe(III)-OIPh are involved in oxidation reactions such as styrene epoxidation[25, 28g]. However, recent experiments utilizing 13-TMC as ligand reveal contrary observations. In the experiment, it has been found that the addition of styrene to the solution of iron(III)-iodosylarene results in the first-order decay product. This suggests the reaction involves a direct attack of oxygen from the iron(III)-iodosylarene. This is supported by various experiments and kinetic isotopic effect (KIE) value of 1.0 suggests the oxygen atom transfer mechanism[11]. Further experiments to probe the mechanistic aspect suggests that *in situ* generated Fe^{IV}=O species using 13-TMC ligand, there were no olefin products. As Fe^{V}=O species are not spectroscopically detected, this also rules out the possibility of this being the oxidant. Collectively all the experiments indicate iron(III)-iodosylarene as a potential oxidant in chemistry, however, there are ambiguities surround to the reactivity of this species compared to very aggressive oxidants such as $Fe^{IV/V}$=O species. Our theoretical studies to probe the relative oxidative abilities of these three species shed light into this mechanistic problems.

First of all, the direct attack of styrene on the iron(III)-iodosylarene (**1**) complex found to have a substantially lower barrier (53.6 kJ/mol). This is associated with the weak I···O bond coupled with relatively stronger Fe-O bond triggering an attack on electron rich olefins. This attack simultaneously cleaves the I···O bond and forms O-C bond leading to a stable cationic intermediate. Absence of axial ligation at the Fe(III) center, strong distortion at the coordination environment lead to strong electrophilic character for the Fe(III)-O(IPh) species. Particularly at the sextet state, oxygen atom found to have a significant spin density (0.24) and this reveals Fe(III)-$O^{\bullet}$ character due to weak I···O bond. This species is electronically equivalent to the oxylradical Fe(III)-$O^{\bullet}$ species which is an electromeric form the putative Fe^{IV}=O species. Thus a

very low barrier for C=C activation is not surprising. The radical character at the ferryl oxygen is not as strong as it is in Fe^{IV}=O and this is triggering two electron transfer leading to the formation of the cationic intermediate, rather than a radical intermediate that is known in Fe^{IV}=O paradigm. Further, the reactant, transition state, and the final intermediate formed all have sextet state ground state and hence no spin-crossover is required for this transformation. The necessity of spin-crossover with Fe(III) species may be a hindrance to its reactivity as Fe(III) species are generally isotropic in nature with very small zero-field splitting – a parameter that can be correlated to the mixing of states and to the feasibility of such spin-crossover. Experimental kinetic data estimate the overall barrier as 30.1 kJ/mol[11], while our estimated barriers are higher than this value, computed energetics are in general agreement with the experiments.

The alternative mechanism involving aggressive oxidants such as $Fe^{IV/V}$=O and this start from the Iron(III)-O(IPh) precursor species where I···O cleavage is expected to be facile. The barrier estimated for the homolytic cleavage of the I···O bond is 51.4 kJ/mol and this is on par to the barrier computed for the activation of olefin. This is a substantial barrier considering a fact that I···O bonds are generally weak. A large barrier is associated with the ligand which is less bulky and sterically less demanding and hence the I···O in this species are found to be shorter than the same computed with different ligand architecture. This is likely to a driving force for such a large kinetic barrier computed. It is worth comparing this barrier to the homolytic cleavage of the I···O bond in [Fe(III)-O(IPh)(Por)(SH)] species reported earlier[25]. For this species, the barriers are estimated to be 33.2, 32.4 and 21.2 kJ for the sextet, quartet and doublet surfaces, respectively. Here doublet surface despite being higher in energy at the reactant found to offer a substantially lower barrier for the I···O bond cleavage, however, this spin-state pathway is completely blocked in 13-TMC ligand architecture. This is likely due to the fact that the π^*_{xz} and π^*_{yz} orbitals are nearly degenerate and there is no strong axial ligand that would destabilize the $s(d_{z^2})$ orbital leading to a unique electronic structure driven by the ligand design. Hence the doublet surface found to lie at 88 kJ/mol in [Fe^{III}-O(IPh)(13-TMC) compared to [Fe^{III}-O(IPh)(Por)(SH)] where it lies at 32.4 k/mol. Absence of the axial ligand also causes the Fe-O and I···O to be shorter and stronger in our case compared to the Cpd-I models studied. All these factors contribute to the barrier leading to the generation of Fe^{IV}=O rather a sluggish process.

Secondly, even if the Fe^{IV}=O species form due to competing nature of the two pathways, our calculations clearly reveal that there is a substantial barrier for the epoxidation reaction by the Fe^{IV}=O species (lowest barrier height estimated at the triplet surface is 32.8 kJ/mol). Again, here as well, the geometry found to play a critical role. As the quintet surface found to be destabilized in this, expected C=C activation solely arise from the triplet state leading to such a sluggish reactivity. This has been witnessed earlier when the equatorial ligands are found to be very strong such as in [(L^{NHC})Fe^{IV}=O] (where L^{NHC} = 3,9,14,20-tetraaza-1,6,12,17-tetraazoniapenta-cyclohexa cosane-1(23),4,6(26),10,12(25),15,17(24),21-octaene) species studied by us and others[12f, 29]. Thus the epoxidation of olefin by the putative Fe^{IV}=O needed a net barrier of 84.2 kJ/mol and this is substantially higher compared to the activation of olefin by the Fe(III)-iodsylarene species. This is clearly substantiated in the experiments where the *in situ* generated Fe^{IV}=O tend to activate C-H bonds leading to hydroxylation product rather than performing oxygen atom transfer reaction.

Formation of Fe^{V}=O from the Fe(III)-iodsylarene is unlikely, as energetics clearly favour homolytic cleavage of the I···O bond. The possibility of donating one electron from the generated Fe^{IV}=O to the reactive PhI cation radical is excessively endothermic and suggests that the presence of Fe^{V}=O is unlikely. All these observations are strongly supported by the experiments[11].

To this end, by studying thoroughly the mechanism of epoxidation of olefin by three different oxidants, our calculations reveal the importance of ligand design and more importantly, how the absence of axial ligand could alter the entire energy landscape of the catalytic transformations. This work unequivocally establishes that Fe(III)-iodsylarene as a potent oxidant. As this is a key catalytic precursor for the formation of Fe^{IV}=O species, this likely to trigger an intense debate on the need to evoke aggressive oxidant such as Fe^{IV}=O in other catalytic transformations.

Conclusions

In present work, DFT calculations have been performed to elucidate the detailed mechanism for the epoxidation of

olefin by the putative Fe^{IV}=O and Fe^{V}=O which are expected to be generated from the catalytic precursor [(13-TMC)Fe^{III}(OIPh)]$^{3+}$ (**1**). Additionally, our work also considers, for the first time, the catalytic precursor as a potent oxidant and attempt to establish the energetic cost associated with the generation of aggressive oxidants vis a vis activation of olefin by the catalytic precursor.

The electronic structure [(13-TMC)Fe^{III}(OIPh)]$^{3+}$ is unique where the π^*_{xz} and π^*_{yz} orbitals are nearly degenerate and $\sigma^*(d_{z^2})$ orbital is stabilized due to the absence of strong donation from the sixth position of the axial ligand. This destabilizes the S = 1/2 state of the precursor complex leading to a substantial difference in reactivity to the known examples. Particularly, S = 1/2 surface known to offer a very low barrier for the I···O bond cleavage and this pathway has a significant energy penalty here with 13-TMC ligand architecture. Stabilization of S = 5/2 as the ground state also eases the energetic requirement for the activation of olefin with the energy penalty of 53.9 kJ/mol leading to epoxidation product.

While calculations rules out the possibility of forming Fe^{V}=O species from the [(13-TMC)Fe^{III}(OIPh)]$^{3+}$ by the heterolytic cleavage of the I···O bond, the homolytic cleavage leading to the formation of Fe^{IV}=O seems viable (51.4 kJ/mol) and the energetics computed are on par with the energy penalty required for the direct epoxidation pathway. However, Fe^{IV}=O species thus generated has substantial kinetic hindrance for the epoxidation of olefins and therefore even if generated, this species unlikely to activate olefins towards oxygen atom transfer reactions. This present rather an interesting conundrum on how the reaction expected to proceed i.e. generation of Fe^{IV}=O or direct epoxidation of olefins by **1**. Given the experimental conditions that substrates are added in excess, epoxidation by species **1** is expected to be a major project as revealed by experiments (65% of products are styrene oxide). All the noted observations are supported by the experiments reported.

Acknowledgements

We thank the Science and Engineering Research Board (CRG/2018/000430) New Delhi, for financial support of this research. A computational facility at Indian Institute of Technology Bombay is greatly acknowledged. RK thanks CSIR for an SRF fellowship. BP would like to acknowledge IIT Bombay and UGC for funding.

Supporting Information

Supporting information contains geometrical parameters of all the species computed, optimized geometries, spin density plots and coordinates of all the species computed.

References

1. (a) M. Costas, M. P. Mehn, M. P. Jensen and L. Que (Jr.), *Chem. Rev.*, 2004, **104**, 939; (b) B. Meunier, S. I. P. de Visser and S. Shaik, *Chem. Rev.*, 2004, **104**, 3947; (c) M. M. Abu-Omar, A. Loaiza and N. Hontzeas, *Chem. Rev.*, 2005, **105**, 2227; (d) I. G. Denisov, T. M. Makris, S. G. Sligar and I. Schlichting, *Chem. Rev.*, 2005, **105**, 2253.
2. (a) B. L. Vallee and R. J. Williams, *Proc. Natl. Acad. Sci. USA*, 1968, **59**, 498; (b) I. Bertini, M. A. Cremonini, S. Ferretti, I. Lozzi, C. Luchinat and M. S. Viezzoli, *Coord. Chem. Rev.*, 1996, **151**, 145; (c) J. M. Boyd, H. Ellsworth and S. A. Ensign, *J. Biol. Chem.*, 2004, **279**, 46644; (d) K. Cho, P. Leeladee, A. J. McGown, S. DeBeer and D. P. Goldberg, *J. Am. Chem. Soc.*, 2012, **134**, 7392; (e) D. C. Lacy, R. Gupta, K. L. Stone, J. Greaves, J. W. Ziller, M. P. Hendrich and A. S. Borovik, *J. Am. Chem. Soc.*, 2010, **132**, 12188.
3. T. Chishiro and Y. Naruta, *Kagaku (Kyoto, Jpn.)*, 2005, **60**, 70.
4. (a) J.-U. Rohde, J.-H. In, M. H. Lim, W. W. Brennessel, M. R. Bukowski, A. Stubna, E. Münck, W. Nam and L. Que, *Science*, 2003, **299**, 1037; (b) F. T. De Oliveira, A. Chanda, D. Banerjee, X. Shan, S. Mondal, L. Que, E. L. Bominaar, E. Münck and T. J. Collins, *Science*, 2007, **315**, 835.
5. (a) M. S. Seo, N. H. Kim, K.-B. Cho, J. E. So, S. K. Park, M. Clemancey, R. Garcia-Serres, J.-M. Latour, S. Shaik and W. Nam, *Chem. Sci.*, 2011, **2**, 1039; (b) S. Shaik, W. Lai, H. Chen and Y. Wang, *Acc. Chem. Res.*, 2010, **43**, 1154.
6. M. R. Bukowski, P. Comba, A. Lienke, C. Limberg, C. Lopez de Laorden, R. Mas Ballesté, M. Merz and L. Que (Jr.), *Angew. Chem., Int. Ed.*, 2006, **45**, 3446.
7. (a) T. Punniyamurthy, S. Velusamy and J. Iqbal, *Chem. Rev.*, 2005, **105**, 2329; (b) S. O. Kim, C. V. Sastri, M. S. Seo, J. Kim and W. Nam, *J. Am. Chem. Soc.*, 2005, **127**, 4178.
8. G. De Faveri, G. Ilyashenko and M. Watkinson, *Chem. Soc. Rev.*, 2011, **40**, 1722.
9. J. T. Groves, T. E. Nemo and R. S. Myers, *J. Am. Chem. Soc.*, 1979, **101**, 1032.
10. (a) C. C. Franklin, R. B. VanAtta, A. F. Tai and J. S. Valentine, *J. Am. Chem. Soc.*, 1984, **106**, 814; (b) Y. Yang, F. Diederich and J. S. Valentine, *J. Am. Chem. Soc.*, 1990, **112**, 7826; (c) B. Meunier, *Chem. Rev.*, 1992, **92**, 1411; (d) H. Tohma and Y. Kita, *Adv. Synth. Catal.*, 2004, **346**, 111; (e) W. Nam, *Acc. Chem. Res.*, 2007, **40**, 522.
11. B. Wang, Y. M. Lee, M. S. Seo and W. Nam, *Angew. Chem., Int. Ed.*, 2015, **54**, 11740.

12. (a) B. Pandey, A. Ansari, N. Vyas and G. Rajaraman, *J. Chem. Sci.*, 2015, **127**, 343; (b) Y. Kang, X.-X. Li, K.-B. Cho, W. Sun, C. Xia, W. Nam and Y. Wang, *J. Am. Chem. Soc.*, 2017, **139**, 7444; (c) B. Pandey, M. Jaccob and G. Rajaraman, *Chem. Commun.*, 2017, **53**, 3193; (d) M. Guo, Y.-M. Lee, M. S. Seo, Y.-J. Kwon, X.-X. Li, T. Ohta, W.-S. Kim, R. Sarangi, S. Fukuzumi and W. Nam, *Inorg. Chem.*, 2018, **57**, 10232; (e) D. Jeong, T. Ohta and J. Cho, *J. Am. Chem. Soc.*, 2018, **140**, 16037; (f) R. Kumar, A. Ansari and G. Rajaraman, *Chem. Eur. J.*, 2018, **24**, 6818.

13. G. W. M. J. T. Frisch, H. B. Schlegel, G. E. Scuseria, M. A. Robb, J. R. Cheeseman, G. Scalmani, V. Barone, B. Mennucci, G. A. Petersson, H. Nakatsuji, M. Caricato, X. Li, H. P. Hratchian, A. F. Izmaylov, J. Bloino, G. Zheng, J. L. Sonnenberg, M. Hada, M. Ehara, K. Toyota, R. Fukuda, J. Hasegawa, M. Ishida, T. Nakajima, Y. Honda, O. Kitao, H. Nakai, T. Vreven, J. A. Montgomery (Jr.), J. E. Peralta, F. Ogliaro, M. Bearpark, J. J. Heyd, E. Brothers, K. N. Kudin, V. N. Staroverov, R. Kobayashi, J. Normand, K. Raghavachari, A. Rendell, J. C. Burant, S. S. Iyengar, J. Tomasi, M. Cossi, N. Rega, N. J. Millam, M. Klene, J. E. Knox, J. B. Cross, V. Bakken, C. Adamo, J. Jaramillo, R. Gomperts, R. E. Stratmann, O. Yazyev, A. J. Austin, R. Cammi, C. Pomelli, J. W. Ochterski, R. L. Martin, K. Morokuma, V. G. Zakrzewski, G. A. Voth, P. Salvador, J. J. Dannenberg, S. Dapprich, A. D. Daniels, Ö. Farkas, J. B. Foresman, J. V. Ortiz, J. Cioslowski, D. J. Fox, Gaussian, Inc., Wallingford CT, 2009.

14. F. Neese, *WIREs Comput. Mol. Sci.*, 2012, **2**, 73.

15. S. Grimme, *Comput. Chem.*, 2006, **27**, 1787.

16. P. J. Hay and W. R. Wadt, *J. Chem. Phys.*, 1985, **82**, 299.

17. (a) A. Schäfer, H. Horn and R. Ahlrichs, *J. Chem. Phys.*, 1992, **97**, 2571; (b) A. Schäfer, C. Huber and R. Ahlrichs, *J. Chem. Phys.*, 1994, **100**, 5829.

18. S. Kozuch and J. M. Martin, *J. Chem. Theory Comput.*, 2013, **9**, 1918.

19. J. Tomasi, B. Mennucci and R. Cammi, *Chem. Rev.*, 2005, **105**, 2999.

20. G. Zhurko and D. Zhurko, *Lite version build*, 2005, **8**, 2005.

21. (a) E. van Lenthe, E.-J. Baerends and J. G. Snijders, *J. Chem. Phys.*, 1994, **101**, 9783; (b) E. v. Lenthe, E.-J. Baerends and J. G. Snijders, *J. Chem. Phys.*, 1993, **99**, 4597.

22. (a) A. E. Reed, R. B. Weinstock and F. Weinhold, *J. Chem. Phys.*, 1985, **83**, 735; (b) A. E. Reed, L. A. Curtiss and F. Weinhold, *Chem. Rev.*, 1988, **88**, 899.

23. T. Z. Gani and H. J. Kulik, *ACS Catalysis*, 2018, **8**, 975.

24. M. Llunell, D. Casanova, J. Cirera, P. Alemany and S. Alvarez, SHAPE, Version 2.1, Universitat de Barcelona, 2013.

25. K. B. Cho, Y. Moreau, D. Kumar, D. A. Rock, J. P. Jones and S. Shaik, *Chem. Eur. J.*, 2007, **13**, 4103.

26. K. B. Wiberg, *Tetrahedron*, 1968, **24**, 1083.

27. (a) E. Manrique, A. Poater, X. Fontrodona, M. Solà, M. Rodríguez and I. Romero, *Dalton Trans.*, 2015, **44**, 17529; (b) A. N. Morozov and D. C. Chatfield, *J. Phys. Chem. B*, 2012, **116**, 12905.

28. (a) D. Kumar, V. S. P. de and S. Shaik, *Chem. Eur. J.*, 2005, **11**, 2825; (b) D. Kumar, E. Derat, A. M. Khenkin, R. Neumann and S. Shaik, *J. Am. Chem. Soc.*, 2005, **127**, 17712; (c) S.-E. Park, W. J. Song, Y. O. Ryu, M. H. Lim, R. Song, K. M. Kim and W. Nam, *J. Inorg. Biochem.*, 2005, **99**, 424; (d) S. P. de Visser, *J. Am. Chem. Soc.*, 2006, **128**, 15809; (e) Y. Suh, M. S. Seo, K. M. Kim, Y. S. Kim, H. G. Jang, T. Tosha, T. Kitagawa, J. Kim and W. Nam, *J. Inorg. Biochem.*, 2006, **100**, 627; (f) J. Bautz, P. Comba, d. L. C. Lopez, M. Menzel and G. Rajaraman, *Angew. Chem., Int. Ed.*, 2007, **46**, 8067; (g) P. Comba and G. Rajaraman, *Inorg. Chem.*, 2007, **47**, 78.

29. (a) F. G. Cantú Reinhard and S. P. de Visser, *Chem. Eur. J.*, 2017, **23**, 2935; (b) C. Kupper, B. Mondal, J. Serrano-Plana, I. Klawitter, F. Neese, M. Costas, S. Ye and F. Meyer, *J. Am. Chem. Soc.*, 2017, **139**, 8939; (c) S. Meyer, I. Klawitter, S. Demeshko, E. Bill and F. Meyer, *Angew. Chem., Int. Ed.*, 2013, **52**, 901.